# Atomistic simulation of fcc–bcc phase transition in single crystal Al under uniform compression*

Li Li(李 莉)[a], Shao Jian-Li(邵建立)[b], Li Yan-Fang(李艳芳)[c], Duan Su-Qing(段素青)[b]†, and Liang Jiu-Qing(梁九卿)[a]

[a] *Institute of Theoretical Physics and Department of Physics, Shanxi University, Taiyuan* 030006, *China*

[b] *Institute of Applied Physics and Computational Mathematics, Beijing* 100088, *China*

[c] *College of Materials Science and Engineering, Taiyuan University of Technology, Taiyuan* 030024, *China*

(Received 28 April 2011; revised manuscript received 23 August 2011)

By molecular dynamics simulations employing an embedded atom model potential, we investigate the fcc-to-bcc phase transition in single crystal Al, caused by uniform compression. Results show that the fcc structure is unstable when the pressure is over 250 GPa, in reasonable agreement with the calculated value through the density functional theory. The morphology evolution of the structural transition and the corresponding transition mechanism are analysed in detail. The bcc (011) planes are transited from the fcc $(11\bar{1})$ plane and the $(1\bar{1}1)$ plane. We suggest that the transition mechanism consists mainly of compression, shear, slid and rotation of the lattice. In addition, our radial distribution function analysis explicitly indicates the phase transition of Al from fcc phase to bcc structure.

**Keywords:** molecular dynamics simulations, phase transition, microstructure

**PACS:** 64.70.Kd, 71.15.Pd, 61.50.Ks **DOI:** 10.1088/1674-1056/21/2/026402

## 1. Introduction

The structural phase stability under high pressure of Al has been studied for more than 30 years. Many experimental or theoretical studies have been performed in this topic. Among these studies, Al has been found to display the fcc-to-hcp or fcc-to-bcc structural phase transition under high pressure.[1−5] Employing the first-principles density functional calculations, Lam and Cohen[2] predicted that the transition pressures of fcc-to-hcp and fcc-to-bcc in Al are at about 200 GPa and 300 GPa, respectively. Mishrab and Chaturvedi[1] indicated that the fcc-to-bcc transition occurs at about 275 GPa. Using the linear combination of Gaussian-type orbitals (LCGTO) technique, Boettger and Trickey[4] compared energies and enthalpies and predicted that the fcc phase should be more stable for pressure below 328 GPa, while the bcc structure is more stable at higher pressure. Very recently, the fcc-to-hcp structural phase transition in Al was investigated by a powder X-ray diffraction experiment.[6] The sample was compressed up to 333 GPa and the fcc-to-hcp phase transition was observed at a reduced volume $V/V_0$ of 0.509, corresponding to a pressure of 217 GPa. Here, $V_0$ is the atomic volume under normal condition. Therefore, the experimentally observed transition pressure result is in general agreement with theoretical predictions.

However, due to the abruptness of the transition process, it is very difficult to observe the atomic scale transition directly in experiment, which brings about the difficulty in theoretically analysing the dynamic response and micro-behaviour of the materials. In recent years, atomistic simulations have been carried out to investigate the phase transition and the corresponding mechanisms in atomic scale.[7−13] In our previous work,[14] we have studied the fcc-to-hcp transition in single crystal Al under uniaxial compression. In this paper, we describe the nucleation and the growth of bcc phase in fcc Al compressed under uniform condition by molecular dynamics (MD) simulations. Our calculations show that the critical pressure of fcc-to-bcc transition is at about 250 GPa, which accords well with previous theoretical predictions.

The rest of the present paper is organized as follows. In Section 2, we briefly explain the method used in our simulation. In Section 3, we give the results of our simulation and the detailed discussion: first,

*Project supported by the Foundations for Development of Science and Technology of China Academy of Engineering Physics (Grant Nos. 2009A0101007 and 2009A0101004).

†Corresponding author. E-mail: duan_suqing@iapcm.ac.cn

© 2012 Chinese Physical Society and IOP Publishing Ltd

we discuss the pressure effect of the phase transition under uniform compression; then, the radial distribution function (RDF) on the transition is evaluated and used to discuss the phase transition; finally, the phase transformation mechanism as well as the microprocess of the nucleation and the growth of new phase are demonstrated. In Section 4 we draw some conclusions from the present study.

## 2. Method of simulation

In the present study, the interaction between atoms is described by an embedded atom model (EAM) potential,[15] which has already been widely used for deformation and phase transition researches of the crystal Al.[14,16,17] We calculate the cold energies of fcc Al, bcc Al and hcp Al by using the above potential, the results are shown in Fig. 1. The intersection points $A$ in Fig. 1(a) and $B$ in Fig. 1(b) indicate that the fcc–bcc and fcc–hcp phase transitions will occur in Al under high pressure. The transition pressures can be obtained by the slope of the tangent of tangential construction between the hcp and bcc in Fig. 1(a) and fcc and hcp phases in Figs. 1(b), which are about 210 GPa and 45 GPa for fcc–bcc and fcc–hcp phase transition, respectively, lower than the results of the first-principles density functional calculations.

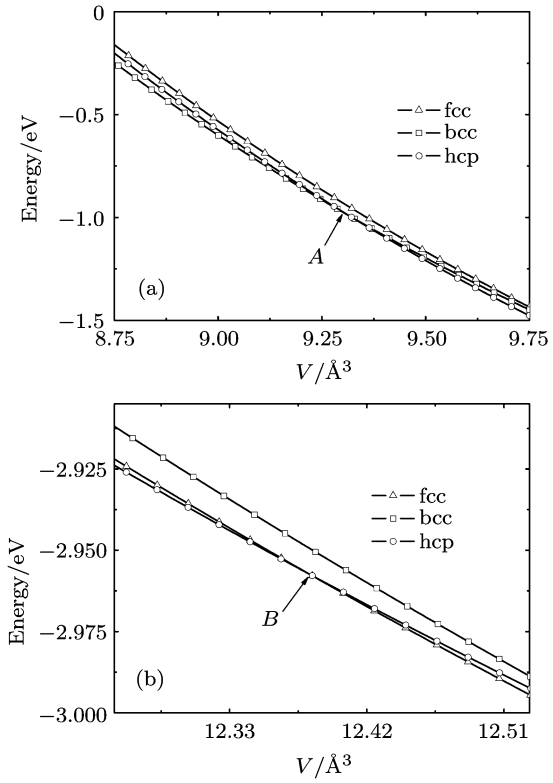



**Fig. 1.** Calculated energies each as a function of atomic volume for fcc Al, bcc Al and hcp Al. The intersection points $A$ [panel (a)] and $B$ [panel (b)] indicate that the fcc–bcc and fcc–hcp phase transitions will occur in Al under high pressure.

In order to explore the phase transition of Al under uniform compression, we construct some fcc single-crystal Al samples. All samples consist of $2.5 \times 10^5$ atoms with different lattice constants for different strains. Periodical boundary conditions are adopted in all the directions. The temperature is set at 300 K by speed calibration method.[18] Relaxing the samples in our MD simulation by using the Verlet algorithm[19] to integrate the equation of motion where the time step is 0.001 ps and the total simulation time is 60 ps. Special techniques are required to analyse a huge number of data produced in the MD simulations. Here, the local structure around each atom is resolved by using the pair analysis technique.[20] The phase mass fraction analysis and the radial distribution functional analysis are also presented to obtain the phase transition information.

## 3. Results and discussion

### 3.1. Pressure analysis

To study the fcc-to-bcc transition under uniform compression, we plot the pressure–time curves for different samples at some constant strains in Fig. 2. Here, the strain $\varepsilon = 1 - V/V_0$ and $V_0$ is the volume of the sample at zero pressure and 300 K with the lattice constant $a_0 = 0.4053$ nm. The time evolutions of the bcc phase mass fraction $\lambda$ under different strains, obtained through the topological pair analysis[20] technique, are shown in Fig. 3. With the increase of uniform compression strain, the following prominent features can be seen from Figs. 2 and 3. Firstly, in strain up to 0.4053 the pressure still behaves calmly and no bcc structure can be found in the whole relaxation process (see Fig. 3). With strain increasing, the sample becomes destabilized. Up to 0.4503, corresponding to a pressure of about 250 GPa, the pressure changes at 2.1 ps and becomes placid at about 20 ps. We can see that the bcc mass fraction changes from 0 to about 0.85 in the relaxing process under this strain. For larger strains, abrupt changes of the pressures are also clear and we do observe the nucleations of the bcc phase in their initial fcc structure in the whole relaxation process. All these performances of the samples indicate that the fcc structure will be unstable when

the pressure is over 250 GPa under uniform compression, which is in reasonable agreement with the value calculated by first-principles; Secondly, when the strain $\varepsilon$ is over 0.4053, the samples are relaxed with constant volumes to approach different pressures and the convergent pressures increasing with the increase of strains; Thirdly, with the increase of strain, the beginning time of the transition, decreases gradually. This can be seen by the points $a$ (0.38 ps, 323.3 GPa), $b$ (0.85 ps, 300.8 GPa), $c$ (1.06 ps, 290.5 Gpa), $d$ (1.4 ps, 279.4 GPa), and $e$ (2.1 ps, 259.5 GPa) respectively on the time–pressure curves in Fig. 2. Finally, we find that the transition time increases as an exponential function with the decrease of pressure. The relationship between transition time and pressure is shown in Fig. 4, where the solid squares denote our simulations and the solid line represents the fitted

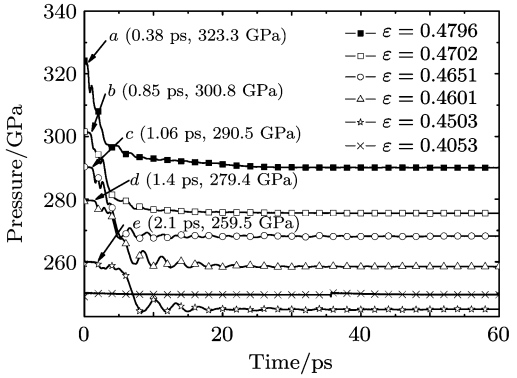



**Fig. 2.** Time evolutions of pressure under constant strains. Points $a$ (0.38 ps, 323.3 GPa), $b$ (0.85 ps, 300.8 GPa), $c$ (1.06 ps, 291.4 GPa), $d$ (1.4 ps, 279.4 GPa), and $e$ (2.1 ps, 259.5 GPa) indicate the beginning of phase transition for constant strains at $\varepsilon = 0.4796$, $\varepsilon = 0.4702$, $\varepsilon = 0.4651$, $\varepsilon = 0.4601$, $\varepsilon = 0.4503$, and $\varepsilon = 0.4053$, respectively.

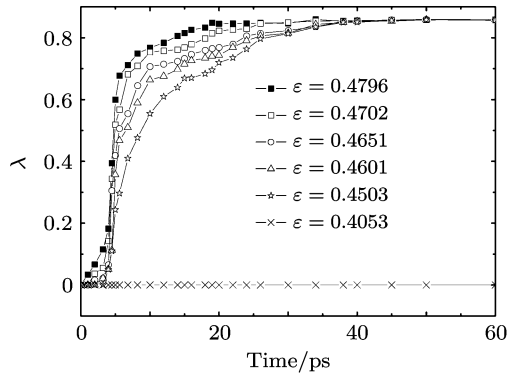



**Fig. 3.** Time evolution of the bcc phase mass fraction $\lambda$ under strains equal to 0.4796, 0.4702, 0.4651, 0.4601, 0.4503, and 0.4053 respectively.

exponential curve. The result here is similar to recent experimental result in iron,[21] where the authors observed the transition time is dependent nonlinearly on the impact pressure in a range of $\sim 1$ ps to $\sim 100$ ns.

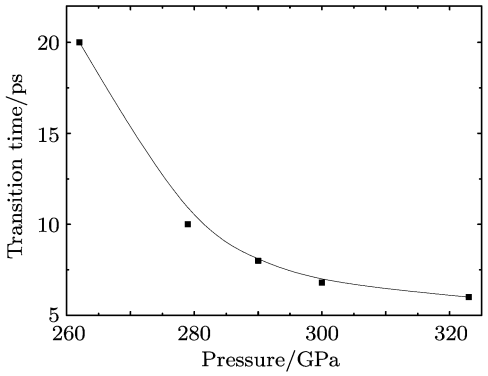



**Fig. 4.** Transition time (solid square) versus pressure obtained by MD simulations. The transition time approximates an exponential function of pressure (solid line).

It should be pointed out that we do not find the fcc–hcp transition in the range of the lower pressure in our work, this may be due to the closer energy of the two phases and the excessive pressure in the contracted samples; in our previous work, the fcc–hcp transition was observed under uniaxial loading due to the effects of the shearing strength.[14,22]

## 3.2. Radial distribution function analysis

In order to describe the fcc–bcc structural phase transition more clearly, the RDFs of the samples under different strains are evaluated and discussed. Corresponding results are displayed in Fig. 5. Obviously, the RDF curves have no change in the relaxing process under strain $\varepsilon = 0.4053$ (see Fig. 5(a)) and the peaks in all curves present typical fcc structure. In other words, the fcc structure is stable when the strain is lower than $\varepsilon = 0.4053$ (corresponding to a pressure of $\sim 250$ GPa). But the situation becomes completely different when the strains exceed the transition critical point. One can see from Figs. 5(b), 5(c), and 5(d) that the RDF curves have distinct changes in relaxation process under the strains $\varepsilon = 0.4503$, 0.4601, and 0.4702. The peaks in the RDF curves become unconspicuous at 5 ps, 3 ps and 2 ps in Figs. 5(b), 5(c), and 5(d), respectively. Notice that the corresponding bcc phase mass fractions in the meantime have changed from 0 to about 0.1 (see Fig. 3). That is to say, the fcc structural phase disappears and the bcc structural phase appears simultaneously at this time. Besides, some new peaks in the RDF curves which represent typical bcc structure emerge at 14 ps, 10 ps and 8 ps, in Figs. 5(b), 5(c), and 5(d), respectively and the peaks become more obvious along with the relaxation

time. In the evening of the relaxing process (time $t = 40$ ps), the RDF curves in Figs. 5(b), 5(c) and 5(d) unfold the typical bcc features. The structures of the samples under strain $\varepsilon = 0.4503$, $\varepsilon = 0.4601$ and $\varepsilon = 0.4702$ have mostly transited from fcc to bcc through enough relaxation. All these features show that the structure of single crystal Al can change from fcc to bcc under uniform compression when the pressure exceeds a critical point.

### 3.3. Nucleation and growth of bcc phase

To have a further insight into how the bcc phase nucleates and grows, the pair analysis technique is used to judge the structural change of the sample. Figure 6 shows the time evolutions of structure morphology of the sample under strain $\varepsilon = 0.4702$. It is clear that the structure of the sample is of fcc phase at the beginning of the relaxation process (Fig. 6(a)). The bcc atoms begin to emerge at 1.2 ps (Fig. 6(c)). Note that the grain boundaries are in (101), (110), and $(0\bar{1}1)$ planes at the beginning of the phase transition process, (which can be seen in Figs. 6(d) and 6(e)), while the (101) plane and the (110) plane are unstable, which will disappear along with the transition process (see Fig. 6(f)). With the relaxation process going on, the bcc phase grows rapidly and nucleates into the main structure gradually in the sample, see Figs. 6(c)–6(e). At the end of the transition process, the sample mainly consists of bcc phase with the boundaries lying in $(0\bar{1}1)$ plane (Fig. 6(f)). Besides, we can see that the grain boundaries separate the sample into three zones (labeled by $Z_1$, $Z_2$, and $Z_3$), see Fig. 6(f). Thereinto, the structural phase transition mechanisms in the three zones are similar, but the nucleation plane in $Z_1$ is different from those in $Z_2$ and $Z_3$. Furthermore, the occurrences of the (101) plane and the (110) plane owe to the shear course in the transition process, all these will be discussed in detail in the next section.

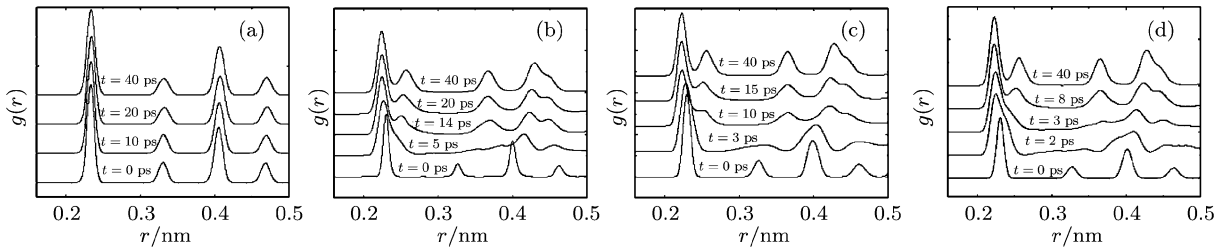



**Fig. 5.** Time evolutions of radial distribution functions (RDFs) for strains $\varepsilon = 0.4053$ (a), $\varepsilon = 0.4503$ (b), $\varepsilon = 0.4601$ (c), and $\varepsilon = 0.4702$ (d).

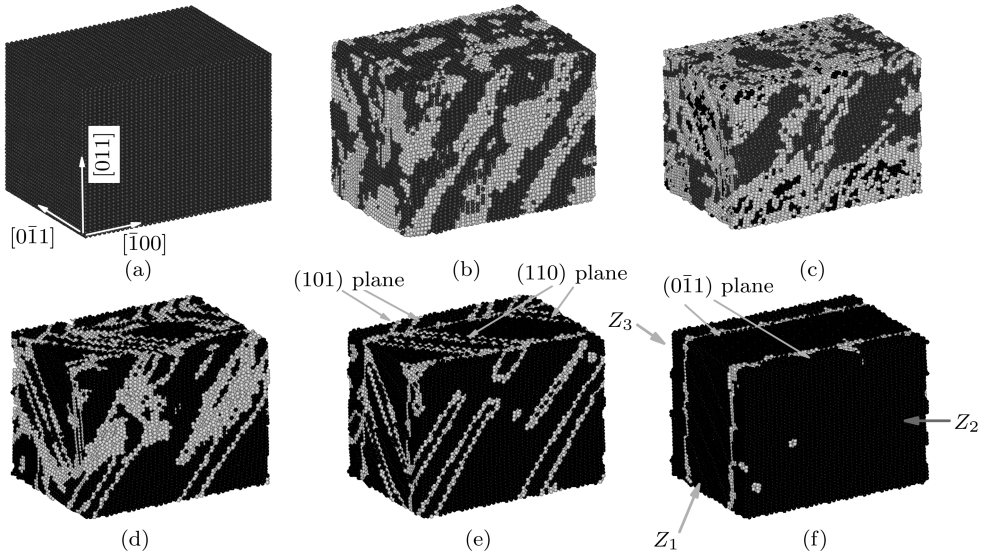



**Fig. 6.** Morphology evolutions of the sample structure under constant strain $\varepsilon = 0.4702$. The panels show the morphologies at different time moments: (a) 0 ps, (b) 1 ps, (c) 1.2 ps, (d) 3 ps, (e) 5 ps, and (f) 20 ps. Deep gray atoms, grayish atoms and black atoms represent fcc phase, grain boundary and bcc phase, respectively.

### 3.4. Transition mechanism analysis

To show the particular procedure of the fcc–bcc phase transition, we perform the microstructural evolution of the atoms from the initial fcc structure to the final bcc structure under strain equals to $\varepsilon = 0.4702$ in Fig. 7. The distance evolutions of the atoms in Fig. 7 are shown in Fig. 8. In addition, figure 9 displays the cross section of the compressed sample relaxed to 20 ps shown in Fig. 6(f). Clearly, it is the fcc $(11\bar{1})$ plane in $Z_1$ and fcc $(1\bar{1}1)$ plane in $Z_2$ and $Z_3$ that transit to the final bcc (011) plane. And the course of the transition contains four main motions: compression, shear, slid and rotation. In $Z_1$, the compression along the $[2\bar{1}1]$ direction and the elongation along the [011] direction can be clearly seen from Figs. 7(b)–7(f). The changes of $d_{57}$ and $d_{69}$ in Fig. 8 quantitatively show these compression and elongation behaviours respectively. In the meantime, the atoms shear along the [010] direction. It is the shear course that brings out the unstable structure — (110) plane in the transition process (see Figs. 6(e) and 9). With the shear course ending, the unstable structure disappears (see Figs. 6(f) and 9). Besides, in Fig. 7, atoms 1, 2, and 3, which belong to fcc $(11\bar{1})$ plane, slid along the $[2\bar{1}1]$ direction with the compression and shear course proceeding. This sliding course can also be seen from the time evolution behaviour of $d_{34}$ in Fig. 8. Therefore, from Figs. 7(a)–7(f) we can see that the structures of the samples have transited from the initial fcc structure to the bcc structure after the compression, shear and sliding courses. Furthermore, our simulation indicates that the transition process also contains a rotation course after the compression, shear and slid courses. The rotation planes are $(11\bar{1})$ planes. As shown in Fig. 7(h), the lattice is rotated by approximately 6.5°. Thus the phase transition is completely finished just after the rotation. In $Z_2$ and $Z_3$,

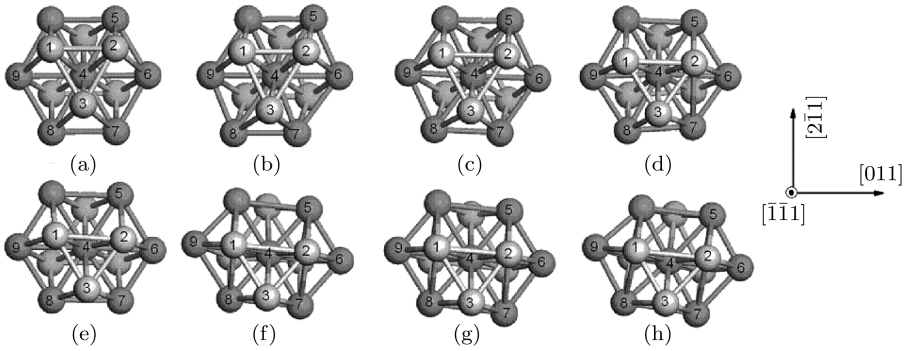



**Fig. 7.** The traces of the atoms under $\varepsilon = 0.4702$, showing the dynamic phase transformation course from the fcc to bcc structure. The time moments for the panels are (a) 0 ps, (b) 1 ps, (c) 2 ps, (d) 3 ps, (e) 4 ps, (f) 5 ps, (g) 6 ps, and (h) 8 ps.

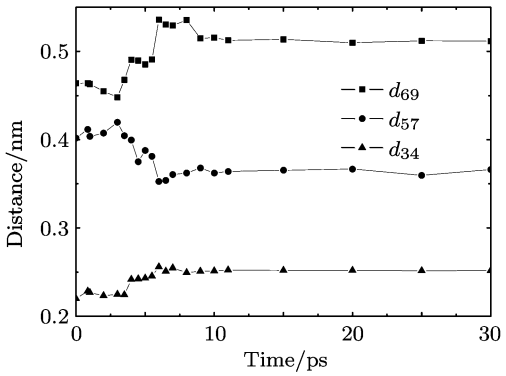



**Fig. 8.** Distance evolutions of the atoms in Fig. 7 under $\varepsilon = 0.4702$. Here, $d_{57}$ shows the distance between atoms 5 and 7 in Fig. 7; $d_{69}$ shows the distance between atoms 6 and 9; $d_{34}$ shows the distance between atoms 3 and 4. While the evolution of $d_{57}$ shows the compression along the $[2\bar{1}1]$ direction and the $d_{69}$ shows the elongation along the [011] direction, the evolution of $d_{34}$ shows the slid procedure.

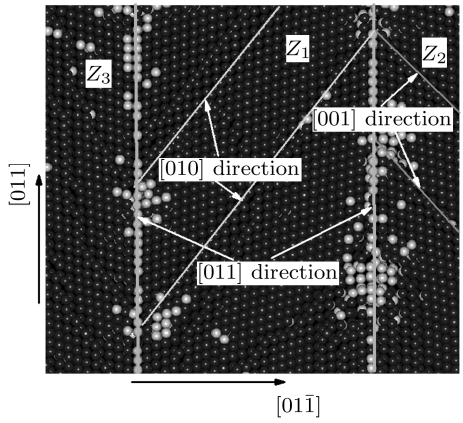



**Fig. 9.** Cross section of the compressed sample relaxed to 20 ps shown in Fig. 6(f). The exceptional arrangement of the atoms which labeled by dash–dot lines and dash lines are brought out by the shear course in the transition process in zones $Z_1$–$Z_3$. Color criterion is the same as that in Fig. 6.

the transition mechanism is similar to that in $Z_1$. In $Z_2$ and $Z_3$, the compression is along the $[21\bar{1}]$ direction and elongation takes place along the [011] direction; the atoms shear along the [001] direction and bring out the unstable structure — (101) plane; the atoms in the $(1\bar{1}1)$ plane slid along the $[21\bar{1}]$ direction. The rotation of the nucleation plane is also found in $Z_2$ and $Z_3$. So we confirm that the fcc–bcc transformation in Al occurs proceeds via the following mechanism. The fcc $(11\bar{1})$ and $(1\bar{1}1)$ planes, which belong to $\{111\}_{\rm fcc}$ family, transit to bcc (011) plane in different zones of the sample; the fcc $(0\bar{1}1)$ planes, which are the interfaces between the two nucleation planes, transit to boundaries after the phase transition. It should be pointed out that a homogeneous nucleation process occurs in the initial stages of the phase transition in our simulation and the new phase grows rapidly along the habit planes. Due to the limitation of size, we find only two habit planes in our simulations. In this paper, we focus on the phase transition mechanism and obtain some informative results. We believe that the basic character of the transition process and the phase transition mechanism are not changed with the limitation of size.

## 4. Conclusions

By using a molecular dynamics method, we successfully simulate the process from fcc to bcc structural phase transition in fcc single crystal Al under hydrostatic compression. The fcc structure is unstable when the pressure is over 250 GPa, which accords well with the value calculated by first-principles. The phase transition occurs on a picosecond time scale and with the increase of pressure the transition relaxation time decreases steadily. The transition time increases as an exponential function with the decrease of the pressure. Our simulation indicates that the phase transition mechanism can be realized through four motions of the lattice: compression, shear, slid and rotation. Atoms in the $[2\bar{1}1]$ direction in $(11\bar{1})$ plane and in the $[21\bar{1}]$ direction in $(1\bar{1}1)$ plane are compressed, atoms in [011] direction are elongated accompanied by a shear course along the [010] direction and the [001] direction respectively. In the mean time, the atoms in the $(11\bar{1})$ plane and the $(1\bar{1}1)$ plane slid along the $[2\bar{1}1]$ direction and the $[21\bar{1}]$ direction respectively. A rotation with about 6.5° of fcc $(11\bar{1})$ and $(1\bar{1}1)$ planes follow on the heels of the above three motions of the lattice. After the four motions, the fcc $(11\bar{1})$ plane and the $(1\bar{1}1)$ plane transit to the bcc (011) plane and the fcc $(0\bar{1}1)$ plane, which are the interfaces between the two nucleating planes and grow to form the boundaries after the phase transition.

## References


[1] Moriarty J A and McMahan A K 1982 *Phys. Rev. Lett.* **48** 809

[2] Lam P K and Cohen M L 1983 *Phys. Rev.* B **27** 5986

[3] Mishra V and Chaturvedi S 2007 *Physica* B **393** 278

[4] Boettger J C and Trickey S B 1996 *Phys. Rev.* B **53** 3007

[5] Tambe M J, Bonini N and Marzari N 2008 *Phys. Rev.* B **77** 172102

[6] Akahama Y, Nishimura M, Kinoshita K and Kawamura H 2006 *Phys. Rev. Lett.* **96** 045505

[7] Kadau K, Germann T C, Lomdahl P S and Holian B L 2002 *Science* **296** 1681

[8] Kadau K, Germann T C, Lomdahl P S and Holian B L 2005 *Phys. Rev.* B **72** 064120

[9] Shao J L, Duan S Q, He A M, Qin C S and Wang P 2009 *J. Phys.*: *Comdens. Matter* **21** 245703

[10] Chen Y X, Xie G F, Ma Y and Zhou Y C 2009 *Acta Phys. Sin.* **58** 4085 (in Chinese)

[11] Cao L X, Shang J X and Zhang Y 2009 *Acta Phys. Sin.* **58** 7307 (in Chinese)

[12] Liang Y C, Liu R S, Zhu X M, Zhou L L, Tian Z A and Liu Q H 2010 *Acta Phys. Sin.* **59** 7930 (in Chinese)

[13] Wang B T, Shao J L, Zhang G C, Li W D and Zhang P 2009 *J. Phys.*: *Condens. Matter* **21** 495702

[14] Li L, Shao J L, Duan S Q and Liang J Q 2010 *New J. Phys.* **12** 033011

[15] Ercolessi F and Adams J B 1994 *Europhys. Lett.* **26** 583

[16] Yamakov V, Wolf D, Phillpot S R, Mukherjee A K and Gleiter H 2002 *Nat. Mater.* **1** 45

[17] Yamakov V, Wolf D, Phillpot S R and Gleiter H 2002 *Acta Mater.* **50** 5005

[18] Hoffmann K H 1996 *Computational Physics* (Berlin: Springer) p. 268

[19] Swope W C andersen H C, Berens P H and Wilson K R 1982 *J. Chem. Phys.* **76** 637

[20] Honeycutt J D and Andersen H C 1987 *J. Phys. Chem.* **91** 4950

[21] Jensen B J, Gray G T III and Hixson R S 2009 *J. Appl. Phys.* **105** 103502

[22] Li L, Shao J L, Duan S Q and Liang J Q 2011 *Chin. Phys.* B **20** 046402